Acta Crystallographica Section A
Foundations of Crystallography
ISSN 0108-7673

Received 1 October 2008
Accepted 16 November 2008

Dynamic Newton–gradient-direction-type algorithm for multilayer structure determination using grazing X-ray specular scattering: numerical simulation and analysis

F. N. Chukhovskii

Institute of Crystallography, Russian Academy of Sciences, 117333 Moscow, Leninsky Prospect 59, Russian Federation. Correspondence e-mail: fchukhov@hotmail.com

A new dynamic iterative algorithm code for retrieving macroscopic multilayer structure parameters (the layer thickness and complex refraction index for each layer, the surface roughness and the interface roughness between the layers) from specular scattering angular scan data is proposed. The use of conventional direct methods, particularly the well known Newton algorithm and gradient-direction-type algorithm operating dynamically to minimize the error functional in a least-squares fashion, is explored. Such an approach works well and seems to be effective in solving the inverse problem in the high-resolution X-ray reflectometry (HRXR) method. In order to demonstrate some features of the proposed iterative algorithm, numerical calculations for retrieving three-layer structure parameters are carried out using simulated HRXR angular scan data. The calculations indicate clearly that the dynamic iterative algorithm is convergent and capable of yielding the true solution. It is important that the performance coefficient for successful iterative cycles for the absolute minimization of the HRXR error functional is quite high even if the initial values of the search parameters are chosen rather far from the true values. It is particularly noteworthy that the relative number of successful iterative cycles is of the order of 90–40% when only moderately accurate initial parameter values, varying by ±10–40% from the true values, are presumed.

1. Introduction

A classical problem in multilayer structure (MLS) physics is the determination of the macroscopic MLS parameters, particularly the thickness, the complex refraction index of each layer, the surface roughness and the interface roughness, with the required accuracy. Such MLS parameters are of interest in applied physics. At present, very few direct methods aimed at determining MLS parameters are self-consistent and provide an unambiguous solution without using prior extra information. Indeed, while methods such as surface X-ray diffraction, absorption X-ray spectroscopy and reflection X-ray fluorescence spectroscopy all work well, each suffers physical limitations since none are sensitive to all the MLS parameters.

Over the last 20 years there has been substantial success using the high-resolution X-ray reflectometry (HRXR) technique coupled appropriately with theoretical model assumptions (see, *e.g.*, Cowley & Ryan, 1987; Sinha *et al.*, 1988; Holy *et al.*, 1999; Asadchikov *et al.*, 1999; Bushuev & Sutyrin, 2000; Bushuev *et al.*, 2002; Lomov *et al.*, 2005; Sutyrin & Prokhorov, 2006; Baake *et al.*, 2006; Bridou *et al.*, 2006; Lemoine *et al.*, 2006; Hodroj *et al.*, 2006).

At present, the most promising method for solving the MLS problem is to decode the one-dimensional HRXR scan data $|R_0^{(\mathrm{ex})}(\theta)|^2$ that result from grazing X-ray specular scattering by an MLS (see Fig. 1, where θ is the grazing angle of the incident X-ray plane-wave radiation). The fundamental theoretical model of grazing X-ray specular scattering by an MLS was developed by Parratt (1954) and is based on sequential Fresnel reflections by each plane layer of the MLS. In a further step, all the partial Fresnel transmission and reflection coefficients are modified by the relevant Debye–Waller transmission term $f_{n-1,n}^{(t)}$ and Debye–Waller reflection term $f_{n-1,n}^{(r)}$ for the interface between the $(n-1)$th and nth layers (Nevot & Croce, 1980). Together they describe the influence of surface and interface roughness on the X-ray specular scattering. This theoretical model has been fruitful in retrieving MLS parameters using the HRXR method in a number of works (Bushuev & Sutyrin, 2000; Bushuev *et al.*, 2002; Sutyrin & Prokhorov, 2006).

There are many diverse iterative methods for solving inverse physical problems, among which one can point out the methods based on the well known Newton and gradient-direction-type algorithms (see, *e.g.*, Press *et al.*, 1992). The Levenberg–Marquardt algorithm (Eadie *et al.*, 1971; Gill *et al.*, 1981; see also Sutyrin & Prokhorov, 2006) is of great interest in

that it represents the direct fusion of the Newton algorithm and a gradient-direction-type algorithm to optimize the iterative procedure itself. Nevertheless, although diverse iterative numerical methods work more or less well and are frequently used, their application to the determination of MLS parameters has not been explored in any detail and needs to be developed further (Sutyrin & Prokhorov, 2006; see also Golberg, 1989). There is virtue in iterative methods that are based upon the minimization of the HRXR error functional $F\{\boldsymbol{P}\}$ as a function of the parameters $\{\boldsymbol{P}\}$ in a least-square fashion. It is noteworthy that the random initial MLS parameters, $\{\boldsymbol{P}^{(\mathrm{start})}\}$, needed to launch the minimization procedure of $F\{\boldsymbol{P}\}$ have to be close to the true parameters, $\{\boldsymbol{P}^{(\mathrm{true})}\}$. This is necessary so as to make the iterative minimization procedure of $F\{\boldsymbol{P}\}$ convergent. From the mathematical and physical viewpoints, the main issue in minimizing the HRXR error functional $F\{\boldsymbol{P}\}$ is to overcome these limitations on the initial MLS parameters.

In this paper, the concept of the Levenberg–Marquardt method is pushed one step further, and it is applied to the retrieval of true MLS parameters using one-dimensional HRXR angular scan data $|R_0^{(\mathrm{ex})}(\theta)|^2$. A prerequisite for solving the problem is to elaborate an appropriate iterative algorithm that achieves the absolute minimization of the HRXR error functional $F\{\boldsymbol{P}\}$ (for reference, the absolute minimum $F\{\boldsymbol{P}^{(\mathrm{true})}\} = 0$) even if the random initial MLS parameter values are chosen rather far away from the true values. The new iterative algorithm has at its core Newton and gradient-direction-type algorithms operating dynamically. The algorithm is convergent and is able to yield the true solution $\{\boldsymbol{P}^{(\mathrm{true})}\}$ without imposing any hard limitations on the random initial MLS parameters $\{\boldsymbol{P}^{(\mathrm{start})}\}$.

For reference, it should be mentioned that choosing the X-ray wavelength λ in the range 0.1–1 nm enables one to detect surface roughness and/or interface roughness in the observed HRXR angular scan data $|R_0^{(\mathrm{ex})}(\theta)|^2$.

In this paper, we are dealing with the true MLS solution using simulated HRXR angular scan $|R_0^{(\mathrm{ex})}(\theta)|^2$ and somewhat arbitrary initial MLS parameters, $\{\boldsymbol{P}^{(\mathrm{start})}\}$, for minimizing the HRXR error functional $F\{\boldsymbol{P}\}$. In place of the known Newton algorithm code and gradient-direction-type algorithms we will use a dynamic iterative algorithm code based on a synthesis of both the Newton and gradient-direction-type algorithms operating dynamically. It appears that no such algorithm for MLS parameter determination has been reported previously.

The iterative algorithm code proposed has been tested on a three-layer structure model based on modified Parratt relationships. The MLS parameters of interest are retrieved using simulated HRXR scan data $|R_0^{(\mathrm{ex})}(\theta)|^2$. It is noteworthy that the dynamic iterative algorithm code clearly indicates a good fit for determining the true MLS parameters. The three-layer structure parameter fitting is controlled by the performance criterion of the dynamic iterative algorithm to achieve the absolute minimum of the HRXR error functional $F\{\mathbf{P}^{(\mathrm{true})}\}$.

2. Theoretical background. The modified Parratt recurrent relationships for an MLS

Before proceeding further, it is important to clarify the mathematical formalism describing a specular component of the grazing X-ray scattering by an MLS. The derivation of the modified Parratt recurrent relationships will be sketched (*cf.* Nevot & Croce, 1980; Bushuev & Sutyrin, 2000; Sutyrin & Prokhorov, 2006). They govern the HRXR reflectivity process by defining sequentially the coefficient $R_0(\theta)$ *via* the appropriate reflectivity coefficients $\{R_n(\theta)\}$ (the integer number n goes from 1 up to N, where N is the total number of layers including the semi-infinite substrate; see Fig. 2).

As shown in Parratt's work (Parratt, 1954), in the case of an *ideally planar* (id) MLS the recurrent relationships take the form

$$R_{n-1}^{(\mathrm{id})} = \frac{r_{n-1,n}^{(0)} + (-r_{n-1,n}^{(0)} r_{n,n-1}^{(0)} + t_{n-1,n}^{(0)} t_{n,n-1}^{(0)}) R_n^{(\mathrm{id})} g_n}{1 + r_{n-1,n}^{(0)} R_n^{(\mathrm{id})} g_n}, \quad (n = 1, 2, \ldots, N). \tag{1}$$

Here $r_{n-1,n}^{(0)}$ is the Fresnel reflection coefficient for the incident X-ray plane wave $\exp[i\mathbf{k}^{(n-1)}\cdot\mathbf{r}]$ propagating within the $(n-1)$th layer medium (note that $r_{n,n-1}^{(0)} = -r_{n-1,n}^{(0)}$),

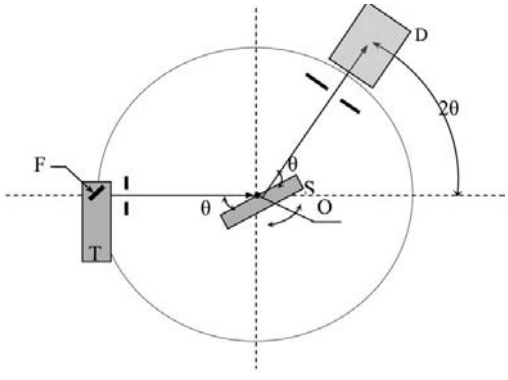

Figure 1
The geometry of the HRXR method. TF is the X-ray source, S is the MLS sample, D is the detector position and θ is the grazing incident angle (the scale is exaggerated).

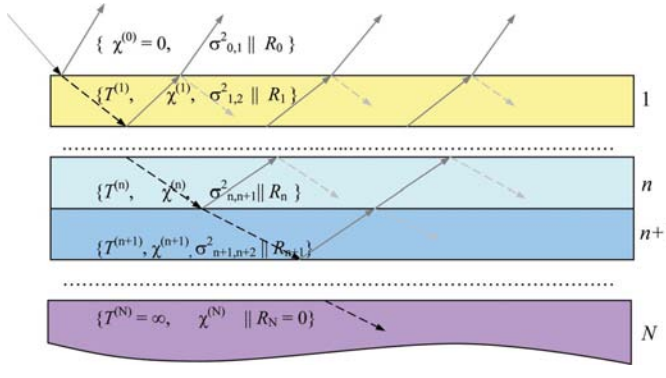

Figure 2
Schematic of an MLS: $T^{(n)}$ and $\chi^{(n)}$ are the thickness and electric susceptibility of the nth layer, $\sigma_{n-1,n}^2$ is the mean-square roughness of the $(n-1, n)$ interface.

$$r_{n-1,n}^{(0)} = \frac{k_z^{(n-1)} - k_z^{(n)}}{k_z^{(n-1)} + k_z^{(n)}} \quad (2)$$

and the exponential factor g_n describes the phase shift due to the plane-wave propagation through the nth layer and is given by

$$g_n = \exp(2ik_z^{(n)} T^{(n)}). \quad (3)$$

Here the normal component of the plane wave $k_z^{(n)}$ within the nth layer medium is defined by

$$k_z^{(n)} = (2\pi/\lambda)(\sin^2\theta + \chi^{(n)})^{1/2}, \quad (4)$$

where λ is the wavelength of the incident X-ray plane wave, $T^{(n)}$ is the nth layer thickness and $\chi^{(n)}$ is the zeroth Fourier component of the complex electric susceptibility $\chi^{(n)}(\mathbf{r})$ of the nth layer medium ($\chi^{(0)} = 0$ for a vacuum).

Accordingly, the Fresnel transmission coefficient $t_{n-1,n}^{(0)}$ can be introduced as $t_{n-1,n}^{(0)} = 1 + r_{n-1,n}^{(0)}$,

$$t_{n-1,n}^{(0)} = \frac{2k_z^{(n-1)}}{k_z^{(n-1)} + k_z^{(n)}}, \quad (5)$$

and the following identity is obtained:

$$-r_{n-1,n}^{(0)} r_{n,n-1}^{(0)} + t_{n-1,n}^{(0)} t_{n,n-1}^{(0)} \equiv 1.$$

By using the basic recurrent relationships [equation (1)] together with equations (2)–(5), and taking into account $R_N^{(\mathrm{id})} = 0$ and $R_{N-1}^{(\mathrm{id})} = r_{N-1,N}^{(0)}$, the self-consistent sequential procedure for calculating the HRXR angular scan $|R_0^{(\mathrm{id})}(\theta)|^2$ for an ideally planar MLS is obtained.

Furthermore, in order to modify the ideal Fresnel coefficients $r_{n-1,n}^{(0)}$ and $t_{n-1,n}^{(0)}$ for a *real model* (ex) of an MLS with a surface roughness and interface roughness in a statistical sense, the Debye–Waller reflection terms and Debye–Waller transmission terms for surfaces and interfaces will be introduced.

For completeness, we shall now exploit the concept of continuous electric wavefields and wavefield derivatives along the normal to each random surface $z_{n-1,n} = u_{n-1,n}(x, y)$ that marks the layer boundary [assuming that each random function $u_{n-1,n}(x, y)$ is smooth and single-valued as well].

Omitting the straightforward calculations, at every point $(x, y, u_{n-1,n})$ one has the following robust equations:

$$\exp(ik_z^{(n-1)}u_{n-1,n}) + r_{n-1,n}\exp(-ik_z^{(n-1)}u_{n-1,n}) = t_{n-1,n}\exp(ik_z^{(n)}u_{n-1,n}), \quad (6a)$$

$$ik_z^{(n-1)}[\exp(ik_z^{(n-1)}u_{n-1,n}) - r_{n-1,n}\exp(-ik_z^{(n-1)}u_{n-1,n})] + \exp(-ik_z^{(n-1)}u_{n-1,n})(\partial r_{n-1,n}/\partial u_{n-1,n}) = ik_z^{(n)} t_{n-1,n}\exp(ik_z^{(n)}u_{n-1,n}) + \exp(ik_z^{(n)}u_{n-1,n})(\partial t_{n-1,n}/\partial u_{n-1,n}). \quad (6b)$$

The following solutions for the Fresnel coefficients $r_{n-1,n}$ and $t_{n-1,n}$

$$r_{n-1,n} = \exp(2ik_z^{(n-1)}u_{n-1,n})r_{n-1,n}^{(0)},$$
$$t_{n-1,n} = \exp[2i(k_z^{(n-1)} - k_z^{(n)})u_{n-1,n}]t_{n-1,n}^{(0)} \quad (7)$$

as functions of the current point $(x, y, u_{n-1,n})$ are easily proven to satisfy equations (6*a*) and (6*b*).

Assuming a function $u_{n-1,n}(x, y)$ to be the Gaussian random variable and its Gaussian distribution as $w(u_{n-1,n}) = (2\pi\sigma_{n-1,n}^2)^{-1/2}\exp[-(u_{n-1,n})^2/2\sigma_{n-1,n}^2]$, one can write down the Debye–Waller reflection term and the Debye–Waller transmission term as follows:

$$f_{n-1,n}^{(r)_{n-1,n}} = \langle\exp(2ik_z^{(n-1)}u_{n-1,n})\rangle = \exp[-2(k_z^{(n-1)})^2\sigma_{n-1,n}^2],$$
$$t_{n-1,n} = \langle\exp[2i(k_z^{(n-1)} - k_z^{(n)})u_{n-1,n}]\rangle = \exp\{-[(k_z^{(n-1)} - k_z^{(n)})^2/2]\sigma_{n-1,n}^2\}, \quad (8)$$

where $\sigma_{n-1,n}^2$ is the mean-square roughness of the $(n-1, n)$th layer boundary.

It should be noted that the above simplified derivation of the static exponential factors [equation (8)] yields the same expressions for the Debye–Waller transmission term as obtained in the pioneering paper of Nevot & Croce (1980), whereas the Debye–Waller reflection term in expressions (8) differs from Nevot & Croce's reflection term of $\exp(-2k_z^{(n-1)}\cdot k_z^{(n)}\sigma_{n-1,n}^2)$. Both the Debye–Waller terms in equation (8) coincide with the corresponding ones introduced in the paper by Bushuev & Sutyrin (2000).

A rigorous theoretical treatment of the static exponential factors is beyond the scope of the present study. However, it is clearly a subject for future theoretical investigation, which might be carried out, for instance, in the frame of Green's function formalism for wavefields propagating through two adjacent media separated by a random surface.

Correspondingly, in the case of the $(n-1, n)$th layer interface modified Fresnel coefficients can be introduced,

$$\hat{r}_{n-1,n} = f_{n-1,n}^{(r)_{n-1,n}} r_{n-1,n}^{(0)},$$
$$\hat{t}_{n-1,n} = f_{n-1,n}^{(t)_{n-1,n}} r_{n-1,n}^{(0)}. \quad (9)$$

Then, repeating the derivation procedure of the recurrent Parratt relationships [equation (1)], each of which is physically based on the sequential reflections and/or transmissions of the plane wavefield due to the nth layer medium, and taking into account the modified Fresnel coefficients $\hat{r}_{n-1,n}, \hat{r}_{n,n-1}$ and $\hat{t}_{n-1,n}, \hat{t}_{n,n-1}$, one can obtain the modified Parratt relationships as [*cf.* Bushuev & Sutyrin (2000) for details]

$$R_{n-1} = \frac{\hat{r}_{n-1,n} + (-\hat{r}_{n-1,n}\hat{r}_{n,n-1} + \hat{t}_{n-1,n}\hat{t}_{n,n-1})R_n g_n}{1 + \hat{r}_{n-1,n}R_n g_n}, \quad (n = 1, 2, \ldots, N). \quad (10)$$

Notice that due to the Debye–Waller factors [equations (8) and (9)] for the modified Fresnel coefficients the identity $-\hat{r}_{n-1,n}\hat{r}_{n,n-1} + \hat{t}_{n-1,n}\hat{t}_{n,n-1} = 1$ does not hold.

The recurrent relationships [equation (10)] together with the physical conditions $R_N = 0$ and $R_{N-1} = \hat{r}_{n-1,n}$ are a starting point for calculating HRXR angular scan $|R_0^{(\mathrm{ex})}(\theta)|^2$ that simulate the grazing X-ray specular scattering by a real MLS within the scope of the statistical MLS model described above.

For the present study, numerous numerical calculations have been carried out for two-layer and three-layer structures.

Using the recurrent relationships [equations (1) and (10)], Figs. 3(*a*) and 3(*b*) show typical examples of the simulated HRXR angular scans $-\ln[|R_0^{(\mathrm{id})}(\theta)|^2]$ and $-\ln[|R_0^{(\mathrm{ex})}(\theta)|^2]$, respectively, for a three-layer structure. Note that the logarithmic scale along the ordinate axes in Figs. 3(*a*) and 3(*b*) is chosen explicitly to reveal peculiarities of the intensities $|R_0^{(\mathrm{id})}(\theta)|^2$ and $|R_0^{(\mathrm{ex})}(\theta)|^2$ outside the total specular reflection region.

Comparison of Figs. 3(*a*) and 3(*b*) clearly displays the combined influence of a surface roughness and interface roughness on the simulated HRXR data under consideration. The smoothing and decreasing effects of the HRXR angular profile oscillations, due to the damping exponential factors of the modified reflection Fresnel coefficients [*cf.* equations (8)], can clearly be seen.

In a further step, the simulated angular scan $|R_0^{(\mathrm{ex})}(\theta)|^2$ depicted on a logarithmic scale in Fig. 3(*b*) will be used to obtain a true solution for the three-layered structure and, in particular, to determine the true MLS structure parameters including the surface roughness and interface roughness.

3. Inverse problem in the HRXR method. Dynamic iterative Newton–gradient-direction-type algorithm

To determine the parameters $\{\boldsymbol{P}\} = \sum_{n=1}^{N}\{P_n\}$, $P_n = (T^{(n-1)}, \chi^{(n-1)}, \sigma^2_{n-1,n})$, that characterize the MLS under consideration, one has to generate the error-functional minimization procedure,

$$F\{\boldsymbol{P}\} = J^{-1}\sum_{j=1}^{J}[|R_0^{(\mathrm{ex})}(\theta_j)|^2 - |R_0(\theta_j;\{P\})|^2]/|R_0^{(\mathrm{ex})}(\theta_j)|^2. \quad (11)$$

In order to minimize the error functional $F\{\boldsymbol{P}\}$ we convert the commonly used Newton and gradient-direction-type algorithms to the modified iterative algorithm, which is purely a synthesis (not a fusion) of the conventional Newton and gradient-direction-type algorithms *operating dynamically*. It is important that each of them is perfectly valid from the mathematical viewpoint. Loosely speaking, *operating dynamically* means that the unique criterion for using either the iterative Newton algorithm or a gradient-direction-type algorithm within the k-iteration process is to provide the minimum value of $F\{\boldsymbol{P}^{(k+1)}\}$ starting from the value of $F\{\boldsymbol{P}^{(k)}\}$ (where k is a successive running number of iterations).

In the case of the iterative algorithm under consideration, passing from the vector $\boldsymbol{P}^{(k)}$ to the vector $\boldsymbol{P}^{(k+1)}$ within the k-iteration process can be cast in the form (the vector differential $\Delta\boldsymbol{P}^{(k)} \equiv \boldsymbol{P}^{(k+1)} - \boldsymbol{P}^{(k)}$)

$$\Delta\mathbf{P}^{(k)} = \Delta\mathbf{P}^{(k)}_{\mathrm{NA}} \cap \Delta\mathbf{P}^{(k)}_{\mathrm{GA}} \quad \text{(the notation } a \cap b \text{ denotes either } a \text{ or } b\text{)}, \quad (12a)$$

where

$$\Delta\mathbf{P}^{(k)}_{\mathrm{NA}} \propto -\hat{\mathbf{H}}[\mathbf{P}^{(k)}]\mathbf{A}[\mathbf{P}^{(k)}] \quad \text{(Newton's algorithm)},$$
$$\Delta\mathbf{P}^{(k)}_{\mathrm{GA}} \propto -\breve{\mathbf{I}}\mathbf{A}[\mathbf{P}^{(k)}] \quad \text{(gradient-direction-type algorithm)}. \quad (12b)$$

Here $\mathbf{P} \equiv \{\mathbf{P}\}$ is the radius vector within the parameter space; $\mathbf{A}(\boldsymbol{P})$ is the gradient vector consisting of the first-order partial derivatives of the error functional $F\{\boldsymbol{P}\}$, $\mathrm{A}_i(\boldsymbol{P}) = \partial F\{\boldsymbol{P}\}/\partial P_i$. $\hat{\mathbf{H}}(\boldsymbol{P})$ is the symmetric Hessian matrix, which is the inverse matrix to the symmetric matrix of the second-order partial derivatives of the error functional $F\{\boldsymbol{P}\}$, namely $\hat{\mathbf{H}}(\boldsymbol{P}) = \hat{\mathbf{G}}^{-1}(\mathbf{P})$, $\hat{G}_{ij}(\mathbf{P}) = \partial^2 F\{\mathbf{P}\}/\partial P_i\,\partial P_j$, and $\breve{\mathbf{I}}$ is a unit matrix.

The flow scheme for the iterative algorithm discussed here looks as follows:

Do[(for a fixed value of n)

– Assign the initial set $\{\boldsymbol{P}\}$ of the structure parameters as

$$P_i^{(\mathrm{start})} = P_i^{(\mathrm{true})}(1 + \Lambda\,\mathrm{Random}[-1, 1]),$$

where Λ is the amplitude (deviation level, $\Lambda < 1$) and the random function Random[−1, 1] gives uniformly distributed pseudo-random real numbers in the range −1 to 1. For each nth cycle the integer iteration number k marking a starting point of the error-functional minimization procedure is equal to zero;

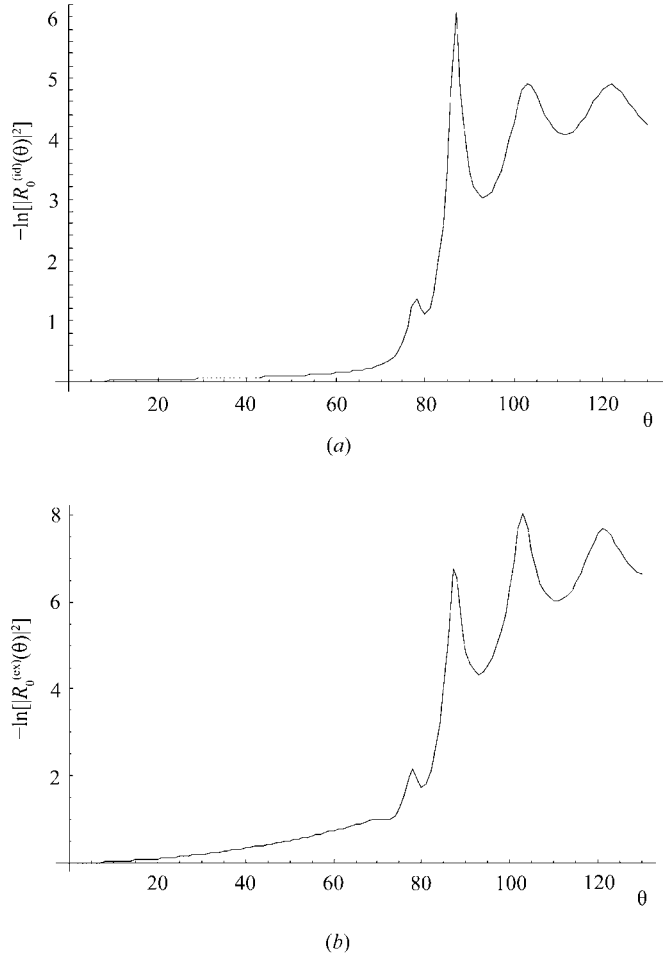

Figure 3
The simulated HRXR angular scans $-\ln[|R_0^{(\mathrm{id})}(\theta)|^2]$ and $-\ln[|R_0^{(\mathrm{ex})}(\theta)|^2]$ *versus* the grazing incident angle θ calculated for the case of a three-layer structure: (*a*) $\sigma^2_{n-1,n} = 0$, (*b*) $\sigma^2_{n-1,n} \neq 0$ (n = 1, 2, 3, 4; see text for details).

Do[(for a fixed value of k)

– Calculate the error functional $F\{\boldsymbol{P}^{(k)}\}$, the gradient vector $\mathbf{A}[\boldsymbol{P}^{(k)}]$ and the second-order partial-derivatives matrices $\hat{\mathbf{G}}[\boldsymbol{P}^{(k)}]$, $\hat{\mathbf{H}}[\boldsymbol{P}^{(k)}] = \hat{\mathbf{G}}^{-1}[\boldsymbol{P}^{(k)}]$;

– Calculate the alternative vector differential of $\pm\Delta\boldsymbol{P}^{(k)}$ in parallel using both the Newton and/or gradient-direction-type formulas (12*a*) and (12*b*) to provide the minimum value of the error functional $F\{\boldsymbol{P}^{(k+1)}\}$. Notice that both the ($\pm$) signs involved in the vector differential of $\pm\Delta\boldsymbol{P}^{(k)}$ for obtaining the minimum value of the error functional $F\{\boldsymbol{P}^{(k+1)}\}$ have to be the same, since according to formulas (12*b*) the vector differential $\Delta\boldsymbol{P}^{(k)}$ defines only the preferable alteration direction of the error functional $F\{\boldsymbol{P}^{(k)}\}$ at the point $\boldsymbol{P}^{(k)}$ to the point $\boldsymbol{P}^{(k+1)}$ and nothing more.

– Calculate the error-functional value $F\{\boldsymbol{P}^{(k+1)}\}$ at the point $\boldsymbol{P}^{(k+1)}$. These values are then fed back in an iterative fashion to the next iteration, $k \rightarrow k+1$;

– Terminate the iterations if the error-functional value $F\{\boldsymbol{P}^{(k+1)}\}$ becomes less than 10^{-9} (the termination value of 10^{-9} is accepted as the absolute minimum of $F\{\boldsymbol{P}^{(\mathrm{true})}\}$).

– Output the final set of $\{\boldsymbol{P}^{(\mathrm{true})}\}$ that have been sought,

– $\{1 \leq k \leq K$, the integer iteration number k runs from 1 up to the total iteration number K; the number k runs for the fixed cycle number $n\}$],

– $\{1 \leq n \leq N$, the integer cycle number n runs from 1 up to the total cycle number $N\}$].

The main difference between the iterative algorithm described here and Levenberg–Marquardt's algorithm (Eadie *et al.*, 1971; Gill *et al.*, 1981; see also Sutyrin & Prokhorov, 2006) is that the latter prescribes the combined single algorithm. The Levenberg–Marquardt algorithm unites both the Newton and gradient-direction algorithms, being in fact the direct fusion of them. Indeed, according to the Levenberg–Marquardt method, for each k-iteration process the vector differential $\Delta\boldsymbol{P}^{(k)}$ is calculated as some linear superposition of $\Delta\boldsymbol{P}^{(k)}_{\mathrm{NA}}$ and $\Delta\boldsymbol{P}^{(k)}_{\mathrm{GA}}$ [*cf.* equations (12*a*) and (12*b*) of the present iterative algorithm].

Our attention is focused in particular on the fact that some important constraints are imposed on the alteration magnitudes $|\Delta P_i^{(k)}|$. Specifically, as found in our case, the peak change $\max[|\Delta P_i^{(k)}|/P_i^{(k)}]$ has to be confined either to a magnitude of the order of 0.05–0.10 or of the order of 0.03 by implementing either Newton's algorithm code or the gradient-direction-type algorithm code, respectively.

Moreover, for the full range of the iteration numbers k none of the calculated parameters $P_i^{(k)}$ are allowed to go out of the range $\pm\Lambda P_i^{(\mathrm{true})}$ around the true values $P_i^{(\mathrm{true})}$.

Loosely speaking, the evolutionary idea of the iterative algorithm described here is to fit the structure parameters $\{\boldsymbol{P}\}$ by dynamically harmonizing Newton's algorithm and the gradient-direction-type algorithm for every iteration number k. The simple idea of uniting the two algorithms so that they operate dynamically as one iterative algorithm is invoked in order to reduce the known problems with the HRXR error-functional minimization procedure. Among these are the problem of the functional slipping towards local minima that give numerous redundant solutions and the problem of minimization-procedure stagnation. These problems increase most when the initial structure parameters that launch the minimization procedure are not close to the true structure parameters.

The dynamic iterative algorithm code described above was tested using simulated HRXR scan data $|R_0^{(\mathrm{ex})}(\theta)|^2$ for a three-layer structure without placing any hard limitations on the initial structure parameters. In the next section, as examples of tests of the dynamic iterative algorithm, some results of the numerical run-through are presented. In the case under consideration the rank of the structure-parameter array $\{\boldsymbol{P}\}$ is equal to 10. How well the dynamic iterative algorithm code worked is controlled by the performance criterion of the relative number of successful iterative cycles to yield the true solution $\{\boldsymbol{P}^{(\mathrm{true})}\}$, which corresponds to the absolute minimum of the error functional $F\{\boldsymbol{P}^{(\mathrm{true})}\} = 0$ provided that the initial parameters $\{\boldsymbol{P}^{(\mathrm{start})}\}$ are randomly defined in a wide range around the true ones.

4. Numerical run-through. Results and discussion

The test case used the simulated input angular scan data $|R_0^{(\mathrm{ex})}(\theta)|^2$ (*cf.* Fig. 3*b*) in order to solve the inverse problem in the HRXR method for a three-layer structure. The other numerical details are $\boldsymbol{P}^{(\mathrm{true})} = \{\{0.80, 0.90, 0.75\}, \{3.0, 4.0, 2.0\}, \{0.211, 0.2285, 0.256, 0.2795\}\}$, where the normalized and/or dimensionless true parameters are listed as follows: from left to right the sequential arrays contain the values of the complex electric susceptibility $(1 - 0.05i)\{\chi^{(4-n)}\}$, the thickness $\{T^{(4-n)}\}$ for $n = 1, 2, 3$ and the mean-square roughness $\{\sigma^2_{4-n,5-n}\}$ for $n = 1, 2, 3, 4$, respectively. For the substrate $\chi^{(4)}$ is assumed to be equal to 1. The thickness $\{T^{(4-n)}\}$ for each n is given in units of $10^{5/2}\lambda/2\pi$; the mean-square roughness of $\{\sigma^2_{4-n,5-n}\}$ for each n is given in units of $10^5(\lambda/2\pi)^2$. The grazing incident angle θ is measured in units of 0.00039 radian, *i.e.* $\theta_j = 0.000039j$, where the integer number j runs from 1 up to J, and J is the rank of the array $\{\theta_j\}$ in which the input angular scan data $|R_0^{(\mathrm{ex})}(\theta_j)|^2$ are calculated.

In order to examine the convergent features of the dynamic iterative algorithm code guiding the procedure for determining the true parameters $\{\boldsymbol{P}^{(\mathrm{true})}\}$, the flow scheme discussed above with the input angular scan data $\{|R_0^{(\mathrm{ex})}(\theta_j)|^2\}$ and diverse initial parameters $\{\boldsymbol{P}^{(\mathrm{start})}\}$ for each cycle n was followed iteratively for the deviation levels $\Lambda = 0.1$, 0.2, 0.3 and 0.4. The total cycle number N was chosen to be 10. The iteration number k runs from 1 up to the total iteration number $K = 220$. For reference, the numerical tests were repeated at least four or five times.

Figs. 4(*a*)–(*d*) show the behavior of the calculated plots of the normalized factor $\bar{E}(\nu) = -\ln[F\{\boldsymbol{P}^{(k_{\mathrm{final}},\nu)}\}/F\{\boldsymbol{P}^{(k_{\mathrm{start}}=0,\nu)}\}]$ *versus* the cycle number $\nu = n + 1$ obtained using the dynamic Newton–gradient-direction-type iterative algorithm detailed above, where the integer cycle number n runs from 1 up to 10 and $\bar{E}(1) \equiv 0$. It is found that the relative number of successful cycles to get the true structure parameters $\{\boldsymbol{P}^{(\mathrm{true})}\}$ are in the range 90–40% while the deviation levels Λ of the initial

structure parameters $\{\boldsymbol{P}^{(\mathrm{start})}\}$ from $\{\boldsymbol{P}^{(\mathrm{true})}\}$ vary from 0.1 up to 0.4. Note that values of the error functional $F\{\boldsymbol{P}^{(\mathrm{true})}\}$ that are less than 10^{-9} contribute to the relative number of successful iteration cycles.

Based on the trends of the $F\{\boldsymbol{P}\}$ reduction behavior observed in Figs. 4(*a*)–(*d*) one can claim that this iterative algorithm code, which uses both Newton's algorithm and a gradient-direction-type algorithm dynamically, provides a good fitting procedure for solving the inverse problem in the HRXR method. The iterative algorithm code presented here governs the error-functional minimization procedure with a high frequency of occurrence of the absolute solution even if the range of the parameters $\{\boldsymbol{P}^{(\mathrm{start})}\}$ is rather wide around $\{\boldsymbol{P}^{(\mathrm{true})}\}$.

5. Concluding remarks

In this paper, the goal of our study was to justify an implementation of the iterative algorithm code detailed above for solving the inverse problem in HRXR. The main feature of the dynamic iterative algorithm code is that it provides a robust unambiguous procedure for determining MLS parameters using HRXR angular scan data and initial MLS parameters without placing any hard limitations upon their starting values. In what is referred to as a general structure-parameter-retrieval problem, the present method is based on a synthesis of two conventional iterative algorithms, Newton's algorithm and a gradient-direction-type algorithm, each of which is widely exploited for HRXR error-functional minimization. The calculated examples presented here indicate that, unlike the iterative methods used before, using the iterative algorithm routinely in a dynamic fashion is reasonable from both physical and mathematical viewpoints and does not depend on strict assumptions about the initial MLS parameters.

The question of how the dynamic parameter-retrieval algorithm works and its application to the extraction of the macroscopic parameters of an MLS using experimentally measured angular scan data $|R_0^{(\mathrm{ex})}(\theta)|^2$, particularly taking into account the experimental counting statistics as well, remains as a good topic for future research.

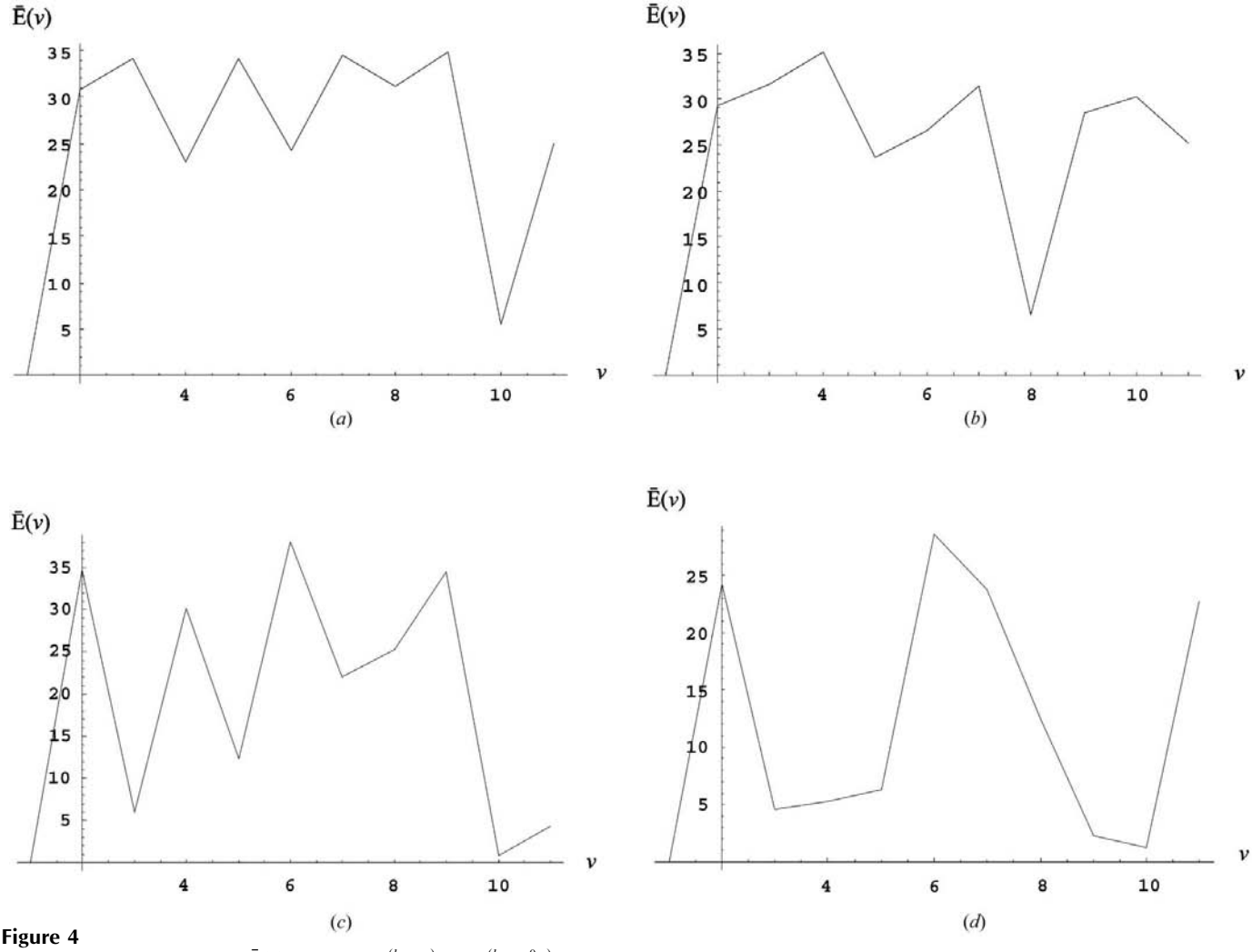

Figure 4
Plot of the normalized factor $\bar{E}(n) = -\ln[F\{\boldsymbol{P}^{(k_{\mathrm{final}},\nu)}\}/F\{\boldsymbol{P}^{(k_{\mathrm{start}}=0,\nu)}\}]$ *versus* the cycle number $\nu = n + 1$. The integer cycle number n runs from 1 up to 10 for the different deviation levels (*a*) $\Lambda = 0.1$, (*b*) $\Lambda = 0.2$, (*c*) $\Lambda = 0.3$, (*d*) $\Lambda = 0.4$. Note that in the case of $\nu = 1$ the iteration number k_{final} is equal to $k_{\mathrm{start}} = 0$ and hence $\boldsymbol{P}^{(k_{\mathrm{final}},1)} = \boldsymbol{P}^{(k_{\mathrm{start}}=0,1)}$, and $\bar{E}(1) \equiv 0$.

With these remarks, we only claim that the iterative algorithm code based on both Newton's algorithm and a gradient-direction-type algorithm operating dynamically is convergent and works well. Let us emphasize once more that how well it will work in practice, in particular using experimental scan data in the HRXR method, remains to be seen and is of interest for future work.

Valuable discussions with and comments from A. M. Poliakov and D. P. Pigorev are gratefully acknowledged.

References

Asadchikov, V. E., Duparre, A., Jakobs, S., Karabekov, A. Yu., Kozhevnikov, I. V. & Krivonosov, Yu. S. (1999). *Appl. Opt.* **38**, 684–691.

Baake, O., Öksüzoglu, R. M., Flege, S., Hoffmann, P. S., Gottschalk, S., Fuess, H. & Ortner, H. M. (2006). *Mater. Charact.* **57**, 12–16.

Bridou, F., Gautier, J., Delmotte, F., Ravet, M.-F., Durand, O. & Modreanu, M. (2006). *Appl. Surf. Sci.* **253**, 12–16.

Bushuev, V. A., Lomov, A. A. & Sutyrin, A. G. (2002). *Crystallogr. Rep.* **47**, 683–690.

Bushuev, V. A. & Sutyrin, A. G. (2000). *Poverkhnost*, **1**, 82–85.

Cowley, R. A. & Ryan, T. W. (1987). *J. Phys. D Appl. Phys.* **20**, 61–67.

Eadie, W. T., Dryard, D., James, F. E., Roots, M. & Saboulet, B. (1971). *Statistical Methods in Experimental Physics.* Amsterdam: North-Holland.

Gill, P. E., Murray, W. & Wright, M. H. (1981). *Practical Optimization.* London: Academic Press.

Golberg, D. E. (1989). *Genetic Algorithms: Search, Optimization and Machine Learning.* New York: Addison-Wesley Publishing Company, Inc.

Hodroj, A., Roussel, H., Crisci, A., Robaut, F., Gottlieb, U. & Deschanvres, J. L. (2006). *Appl. Surf. Sci.* **253**, 363–366.

Holy, V., Pietsch, U. & Baumbach, T. (1999). *High-Resolution X-ray Scattering from Thin Films and Multilayers.* Berlin: Springer Verlag.

Lemoine, P., Quinn, J. P., Maguire, P. D. & McLaughlin, J. A. D. (2006). *Carbon*, **44**, 2617–2624.

Lomov, A. A., Sutyrin, A. G., Prokhorov, D. Yu., Galiev, G. B., Khabarov, Yu. V., Chuev, M. A. & Imamov, R. M. (2005). *Crystallogr. Rep.* **50**, 739–750.

Nevot, L. & Croce, P. (1980). *Rev. Phys. Appl.* **15**, 761–779.

Parratt, L. G. (1954). *Phys. Rev.* **95**, 359–369.

Press, W. H., Flannery, B. P., Teukolsky, S. A. & Vetterling, W. T. (1992). *Numerical Recipes in C: The Art of Scientific Computing*. Cambridge University Press.

Sinha, S. K., Sirota, E. B., Garoff, S. & Stanley, H. B. (1988). *Phys. Rev. B*, **38**, 2297–2311.

Sutyrin, A. G. & Prokhorov, D. Yu. (2006). *Crystallogr. Rep.* **51**, 570–576.